Journal of Alloys and Compounds 514 (2012) 64–70

Contents lists available at SciVerse ScienceDirect

Journal of Alloys and Compounds

journal homepage: www.elsevier.com/locate/jallcom

Crystal growth, structure, and physical properties of Ln_2PdGa_{12} (Ln = La, Pr, Nd, and Sm)

Michael J. Kangas[a], Brenton L. Drake[a], Neel Haldolaarachchige[b], D.P. Young[b], Julia Y. Chan[a,*]

[a] Department of Chemistry, Louisiana State University, Baton Rouge, LA 70803, USA
[b] Department of Physics and Astronomy, Louisiana State University, Baton Rouge, LA 70803, USA

ARTICLE INFO

Article history:
Received 28 September 2011
Received in revised form 21 October 2011
Accepted 24 October 2011
Available online 10 November 2011

Keywords:
Intermetallics
Rare earth alloys and compounds
Crystal growth
Heat capacity
Heavy fermions
Magnetization

ABSTRACT

Single crystals of Ln_2PdGa_{12} (Ln = La, Pr, Nd, Sm) were synthesized with a molten Ga flux. The intermetallic phases are isostructural to Sm_2NiGa_{12} with cell dimensions of $a \sim 6.1$ Å and $c \sim 15.5$ Å. Pr_2PdGa_{12}, Nd_2PdGa_{12}, and Sm_2PdGa_{12} order antiferromagnetically at 18, 7.5, and 7.5 K, respectively, and magnetic properties of single crystals oriented parallel and perpendicular to the magnetic field are presented. Fitting the low temperature heat capacity of Pr_2PdGa_{12} gives a Sommerfeld coefficient (γ) of 250 mJ mol^{-1} K^{-2} and indicates the possibility of heavy fermion behavior.

Published by Elsevier B.V.

1. Introduction

The competition of interactions in highly correlated systems can lead to new and interesting phenomena. These interactions can be tuned by changing temperature, field, pressure, or chemical doping. Compounds adopting the $HoCoGa_5$ structure type [1] provide a number of remarkable examples. These include the heavy fermion superconductors $CeCoIn_5$ [2] and $CeIrIn_5$, and the antiferromagnetic superconductor $CeRhIn_5$ [3]. The discovery of these phases led our group to investigate whether similar phases could be found in the Ce–Pd–Ga phase space. Three new phases were discovered: $CePdGa_6$ [4], Ce_2PdGa_{12} [5], and Ce_2PdGa_{10} [6]. All three structure types are tetragonal and can be described as layers of cerium and gallium resembling those found in the $HoCoGa_5$ structure type compounds [1]. $CePdGa_6$ and Ce_2PdGa_{12} are heavy fermion antiferromagnets with $\gamma \sim 300$ mJ mol^{-1} K^{-2} ($T_N = 10$ K) and $\gamma \sim 72$ mJ mol^{-1} K^{-2} ($T_N = 11$ K), respectively. Heavy fermions are compounds where conduction electrons interact strongly with local magnetic moments and thus behave as if they have increased electron mass. A large ($\gamma > 100$ mJ mol^{-1} K^{-2}) Sommerfeld parameter is a characteristic of these materials and is determined by fitting low-temperature heat capacity to $C = \gamma T + \beta T^3$, where βT^3 is the phonon contribution to the specific heat. Ce_2PdGa_{10} does not show any magnetic ordering down to 2 K; however, it shows a positive 200% change in magnetoresistance in a 9-T field.

Further studies were conducted on Ce_2NiGa_{12} and Ce_2CuGa_{12} to determine the role the transition metal plays in the physical properties. The nickel analogue is a moderate heavy fermion ($\gamma \sim 191$ mJ mol^{-1} K^{-2}) and also displays antiferromagnetic ordering, while the copper analogue does not show magnetic ordering down to 2 K, and the electron mass is less enhanced ($\gamma \sim 69$ mJ mol^{-1} K^{-2}) [7]. Investigation of the phases Ln_2MGa_{12} (Ln = Pr, Nd, Sm and M = Cu, Ni) show antiferromagnetic order between 3 and 18 K, with Nd_2NiGa_{12} showing the highest ordering of the nickel series, and Nd_2CuGa_{12} having the lowest ordering of the copper series. However, we note that in the copper analogues, occupancies on the transition metal sites decrease going from Ce to Sm [8].

Many cerium-, ytterbium-, and uranium-containing heavy fermion compounds have been discovered. However, relatively few heavy fermion compounds have been discovered for the lanthanides Pr, Nd, and Sm [9]. Notable Pr heavy fermions include $Pr(Cu,Ga)_{13-x}$ ($\gamma \sim 100$ mJ mol^{-1} K^{-2}) [10], $PrOs_4Sb_{12}$ ($\gamma \sim 500$ mJ mol^{-1} K^{-2}) [11], $Pr_2Rh_3Ge_5$ ($\gamma \sim 80$ mJ mol^{-1} K^{-2}) [12], and $PrInAg_2$ ($\gamma \sim 6500$ mJ mol^{-1} K^{-2}) [13]. Unlike Ce and U compounds, where valence instability correlates with heavy fermion behavior, the trivalent Pr materials are stable, and the enhanced electron mass has been attributed to quadrupolar-Kondo interactions or the interaction of a low-lying excited state [12–14]. Herein we report the synthesis, structure, and the physical properties of Pr_2PdGa_{12}, Nd_2PdGa_{12}, and Sm_2PdGa_{12}.

* Corresponding author. Tel.: +1 225 578 2695; fax: +1 225 578 3458.
E-mail address: jchan@lsu.edu (J.Y. Chan).

0925-8388/$ – see front matter. Published by Elsevier B.V.
doi:10.1016/j.jallcom.2011.10.086

2. Experimental

2.1. Synthesis

Single crystals of La_2PdGa_{12}, Pr_2PdGa_{12}, Nd_2PdGa_{12}, and Sm_2PdGa_{12} were grown in the presence of excess Ga flux [15]. Ln (3N, chunks, Alfa Aesar), Pd (4.5N, powder, Alfa Aesar) and Ga (7N, pellets, Alfa Aesar) were used as received and were placed in alumina crucibles with a reaction ratio of 1.5:1:15 for Ln:Pd:Ga. Each crucible was loaded into a fused silica tube and the contents evacuated (0.05–0.07 mmHg) and sealed. The samples were placed into a furnace and heated to a dwell temperature of 1150 °C for 7 h at 170 °C/h. The samples were then rapidly cooled (150 °C/h) to 500 °C followed by slow cooling to 400 °C at a rate of 8 °C/h. The samples were then inverted and centrifuged to separate the single crystals from excess Ga flux. Residual flux on the surface of the crystals was removed by sonicating in hot water or etching with a solution of iodine in dimethylformamide (3 M). Etched crystals were thin silver plates of ~1–2 mm^2. Single crystals were mechanically separated based on morphology and were ground and characterized by powder X-ray diffraction and the data show that the sample is indeed homogeneous and single phase. Attempts to extend the series to Gd with the same reaction conditions were unsuccessful and resulted in the formation of the Gd_4PdGa_{12} which crystallizes in the Y_4PdGa_{12} structure type [16].

2.2. X-ray diffraction and elemental analysis

For each compound, a suitable crystal of approximately 0.05 mm × 0.05 mm × 0.05 mm were cut and mounted to the tip of a glass fiber using epoxy. They were then positioned onto the goniometer of a Nonius Kappa diffractometer. Diffraction data were collected at 298 K with Mo K_α radiation (λ = 0.71073 Å). Further crystallographic parameters for Ln_2PdGa_{12} (Ln = La, Pr, Nd, and Sm) are provided in Table 1. The crystal structure was solved with direct methods using SIR97 to give a starting model and refined with SHELXL97 [17,18]. Structural refinement included extinction and anisotropic atomic displacement parameters. The extinction coefficient for the La analogue was subsequently removed as it was not statistically significant. Attempts to refine the occupancy of each atomic position individually resulted in nearly 100% occupancy of each site, and all sites were treated as fully occupied in the final model. In addition, an attempt to split the Ga4 site into two partially occupied sites, as observed in La_2CuGa_{12} [7], resulted in minimal occupancy (~5%) of the minority site and was not considered in the final model. Atomic positions and displacement parameters are presented in Table 2, and selected interatomic distances are provided in Table 3. The 0 0 1 reflection was found to be obstructed by the X-ray beam stop in the Pr, Nd, and Sm analogues and was omitted from the final model.

The composition was confirmed using energy dispersive spectroscopy (EDS) on a Hitachi S-3600N variable-pressure scanning electron microscope equipped with an energy-dispersive spectrometer. The accelerating voltage was 15 kV with a beam-to-sample distance of 15 mm. An average of 15–20 scans was performed on each single crystal. The compositions determined by EDS and normalized to the lanthanide were $La_{2.00}Pd_{1.13(7)}Ga_{11.71(11)}$, $Pr_{2.00}Pd_{1.04(4)}Ga_{11.59(5)}$, $Nd_{2.00}Pd_{0.94(7)}Ga_{11.44(12)}$, and $Sm_{2.00(4)}Pd_{0.96(7)}Ga_{11.42(8)}$, and are in excellent agreement with the models from the single crystal X-ray diffraction refinement.

2.3. Physical properties

Single crystals were selected for physical property measurements were first characterized by X-ray diffraction and energy dispersive spectroscopy. Magnetic data were collected using a Quantum Design Physical Property Measurement System (PPMS). The temperature-dependent susceptibility data were measured under zero-field cooled (ZFC) conditions between 3 K and 300 K for Ln_2PdGa_{12} (Ln = Pr–Sm). Pr and Nd were each measured under an applied field of 0.1 T, and Sm_2PdGa_{12} was measured under an applied field of 4 T. Field-dependent magnetization data were measured at 3 K with applied fields up to 9 T. The electrical resistivity measurements were measured on single crystals by the standard four-probe AC technique. The heat capacity was measured by the standard adiabatic heat-pulse relaxation technique down to 0.4 K.

3. Results and discussion

3.1. Structure

Ln_2PdGa_{12} (Ln = Pr, Nd, or Sm) are isostructural to Sm_2NiGa_{12} [19] and adopt the space group $P4/nbm$ with $a \sim 6.1$ Å and $c \sim 15.5$ Å. The lanthanide contraction can be observed in the decrease in unit cell volume as well as the a and c lattice parameters with c/a ratios of 2.534(1), 2.554(1), 2.559(1), 2.564(1) for La, Pr, Nd, and Sm, respectively. The crystal structure has been previously described as a Ga–Pd network with lanthanide atoms occupying cavities in the network [19] (Fig. 1). The Ln atoms reside in a cavity formed by 14 Ga atoms with Pr–Ga distances of ~3.2–3.3 Å. The Pd–Ga segment is comprised of edge-sharing rectangular prisms formed from 4 Ga3 atoms at 2.5495(9) Å and another 4 Ga3 atoms at 2.5534(9) Å in Pr_2PdGa_{12}.

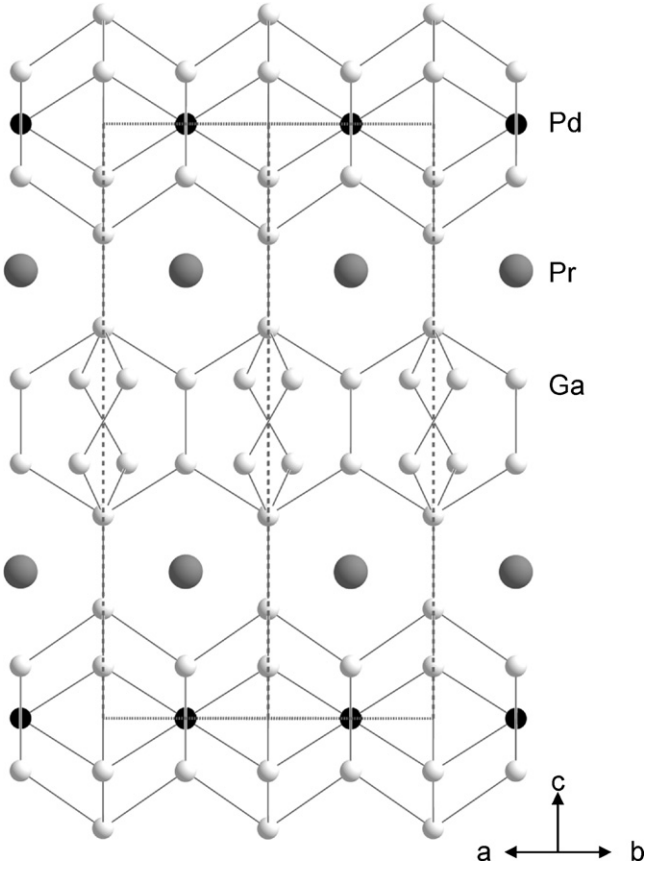

Fig. 1. The crystal structure of Pr_2PdGa_{12} is shown. Pr, Pd, and Ga atoms are represented as large gray, black, and small gray spheres, respectively.

3.2. Physical properties

Fig. 2a and b shows the temperature dependent molar magnetic susceptibility (χ_m) of single crystals Ln_2PdGa_{12} (Ln = Pr, Nd, and Sm) with magnetic field parallel and perpendicular to the direction of the plate. Anisotropic field-dependent magnetization data at T = 3 K for all analogues are shown in Fig. 3a and b. All analogues were fit with a modified Curie–Weiss equation in the form of $\chi(T) = \chi_0 + C/(T - \theta)$, where C is the Curie constant, θ_W is the Weiss temperature, and χ_0 is a constant representing the background contribution to the magnetic susceptibility. In all cases, the modified Curie–Weiss equation was fit over the linear region of $1/[\chi(T) - \chi_0]$ and Table 4 provides the fit range, θ, μ_{calc}, and μ_{eff}.

3.2.1. Magnetic susceptibility and magnetization of Ln_2PdGa_{12} (Ln = Pr, Nd, and Sm)

Fig. 2a shows the molar magnetic susceptibility of Pr_2PdGa_{12} down to 3 K with H parallel to the c-axis of the plate. Pr_2PdGa_{12} undergoes a very sharp antiferromagnetic transition at 18 K for H = 0.1 T. At low temperature the value of the magnetic susceptibility is less than the room-temperature value, indicating that the parallel component of the spins is exactly aligned with the crystal c-axis (and thus the applied field). Fig. 2b shows the molar magnetic susceptibility of Pr_2PdGa_{12} down to 3 K with H parallel to the ab-plane of the crystal. A modest decease in x, as T decreases, is present at 18 K, and could be caused by imperfect alignment of the crystal

Table 1
Crystallographic parameters.

Compound	La_2PdGa_{12}	Pr_2PdGa_{12}	Nd_2PdGa_{12}	Sm_2PdGa_{12}
Crystal system	Tetragonal	Tetragonal	Tetragonal	Tetragonal
Space group	*P*4/*nbm*	*P*4/*nbm*	*P*4/*nbm*	*P*4/*nbm*
a (Å)	6.1550(9)	6.0870(6)	6.0680(12)	6.0480(12)
c (Å)	15.594(2)	15.547(2)	15.531(2)	15.5100(16)
V (Å^3)	590.76(15)	576.04(11)	571.86(18)	567.33(17)
Z	2	2	2	2
Crystal dimensions (mm^3)	0.03 × 0.05 × 0.05	0.08 × 0.08 × 0.08	0.08 × 0.08 × 0.08	0.05 × 0.08 × 0.08
θ range (°)	2.61–30.01	2.62–29.96	2.62–30.04	2.63–30.04
μ (mm^{-1})	35.331	37.275	38.107	39.61
Data collection				
Measured reflections	1572	1454	1283	1327
Independent reflections	497	477	479	478
Reflections with $I > 2\sigma(I)$	409	453	325	389
R_{int}	0.0333	0.0265	0.1052	0.0647
h	−8 to 8	−8 to 8	−8 to 8	−8 to 8
k	−8 to 8	−6 to 6	−6 to 6	−6 to 6
l	−21 to 21	−21 to 19	−21 to 16	−21 to 16
Refinement				
R_1[a]	0.0354	0.0349	0.043	0.0309
wR_2[b]	0.0848	0.1096	0.0937	0.0795
Reflections	497	477	479	478
Parameters	25	26	26	26
$\Delta\rho_{max}$(e$^-$/Å^3)	5.163	4.21	2.432	2.631
$\Delta\rho_{min}$(e$^-$/Å^3)	−2.12	−2.308	−2.126	−1.546
Extinction coefficient	–	0.0022(4)	0.0034(4)	0.0045(4)
GoF	1.078	1.355	1.016	1.078

[a] $R_1 = \sum ||F_o| - |F_c|| / \sum |F_o|$.

[b] $R_w = [\sum [w(F_o^2 - F_c^2)^2] / \sum [w(F_o^2)^2]]^{1/2}$; $w = 1/[\sigma^2(F_o^2) + (0.0410P)^2 + 7.0512P]$, $w = 1/[\sigma^2(F_o^2) + (0.00561P)^2 + 5.0173P]$, $w = 1/[\sigma^2(F_o^2) + (0.0404)^2]$, and $w = 1/[\sigma^2(F_o^2) + (0.0354P)^2 + 2.7132P]$, respectively, for La_2PdGa_{12}, Pr_2PdGa_{12}, Nd_2PdGa_{12}, and Sm_2PdGa_{12}.

resulting in some contribution from the *c*-direction. Inverse molar magnetic susceptibility (not shown), in each direction, is consistent with Curie–Weiss like behavior at temperatures greater than 30 K. Fitting above this temperature with a modified Curie–Weiss equation, θ_W and μ_{eff} were found to be 10.1(2) K and 3.64(1)μ_B/mol Pr for the field parallel to the *c*-axis and −21.5(5) K and 3.61(3)μ_B/mol Pr for the field parallel to the *ab*-plane. The magnetic moment from the high temperature Curie–Weiss fits is in good agreement with the calculated moment of a Pr^{3+} ion (3.58μ_B/Pr). The positive Weiss temperature, along the *c*-direction, is indicative of ferromagnetic coupling between spins. Previous reports on Ce_2PdGa_{12} indicate that the spins are ferromagnetically coupled in the *ab*-plane and

Table 2
Atomic positions and atomic displacement parameters.

Site	Wyckoff	Symmetry	*x*	*y*	*z*	U_{eq}[a]
La_2PdGa_{12}						
La1	4*h*	*mm*	3/4	1/4	0.24638(4)	0.0089(2)
Pd1	2*c*	−42*m*	3/4	1/4	0	0.0095(3)
Ga1	4*g*	4	3/4	3/4	0.18229(9)	0.0107(3)
Ga2	4*g*	4	3/4	3/4	0.34073(9)	0.0139(3)
Ga3	8*m*	*m*	0.50009(11)	0.00009(11)	−0.08677(6)	0.0107(3)
Ga4	8*m*	*m*	0.5649(2)	0.0649(2)	0.42782(8)	0.0325(4)
Pr_2PdGa_{12}						
Pr1	4*h*	*mm*	3/4	1/4	0.24665(4)	0.0069(3)
Pd1	2*c*	−42*m*	3/4	1/4	0	0.0069(3)
Ga1	4*g*	4	3/4	3/4	0.18459(9)	0.0082(4)
Ga2	4*g*	4	3/4	3/4	0.34209(9)	0.0111(4)
Ga3	8*m*	*m*	0.50027(10)	0.00027(10)	−0.08816(6)	0.0082(3)
Ga4	8*m*	*m*	0.57215(14)	0.07215(14)	0.42893(7)	0.0191(4)
Nd_2PdGa_{12}						
Nd1	4*h*	*mm*	3/4	1/4	0.24688(7)	0.0104(3)
Pd1	2*c*	−42*m*	3/4	1/4	0	0.0103(5)
Ga1	4*g*	4	3/4	3/4	0.18521(15)	0.0109(5)
Ga2	4*g*	4	3/4	3/4	0.34224(15)	0.0143(5)
Ga3	8*m*	*m*	0.50024(17)	0.00024(17)	−0.08854(10)	0.0117(4)
Ga4	8*m*	*m*	0.5740(2)	0.0740(2)	0.42911(13)	0.0231(5)
Sm_2PdGa_{12}						
Sm1	4*h*	*mm*	3/4	1/4	0.24678(5)	0.0066(2)
Pd1	2*c*	−42*m*	3/4	1/4	0	0.0067(3)
Ga1	4*g*	4	3/4	3/4	0.18634(11)	0.0073(3)
Ga2	4*g*	4	3/4	3/4	0.34273(11)	0.0106(3)
Ga3	8*m*	*m*	0.50019(11)	0.00019(11)	−0.08909(7)	0.0079(3)
Ga4	8*m*	*m*	0.57592(13)	0.07592(13)	0.42918(8)	0.0168(3)

[a] U_{eq} is defined as one-third of the trace of the orthogonalized U_{ij} tensor.

Table 3
Selected interatomic distances (Å).

Compound	La_2PdGa_{12}	Ce_2PdGa_{12}[a]	Pr_2PdGa_{12}	Nd_2PdGa_{12}	Sm_2PdGa_{12}
Ln layer					
Ln-Ga1 (x4)	3.2357(7)	3.2033(5)	3.1928(6)	3.1816(10)	3.1660(8)
Ln-Ga4 (x2)	3.2561(14)	3.2286(13)	3.2210(12)	3.208(2)	3.1969(14)
Ln-Ga3 (x2)	3.3056(11)	3.2772(11)	3.2701(10)	3.2621(18)	3.2476(12)
Ln-Ga3 (x2)	3.3066(11)	3.2808(11)	3.2731(10)	3.2649(18)	3.2498(12)
Ln-Ga2 (x4)	3.4112(8)	3.3914(11)	3.3859(7)	3.3762(12)	3.3703(10)
$PdGa_6$ segment					
Ga1-Ga3 (x4)	2.6371(10)	2.6257(10)	2.6228(9)	2.6185(16)	2.6168(12)
Pd-Ga3 (x4)	2.5618(10)	2.5512(10)	2.5495(9)	2.5465(15)	2.5445(11)
Pd-Ga3 (x4)	2.5631(10)	2.5558(10)	2.5534(9)	2.5500(15)	2.543(11)
Ga-only segment					
Ga2-Ga4 (x4)	2.6265(11)	2.6173(10)	2.6153(10)	2.6126(16)	2.6061(12)
Ga4-Ga4 (x1)	2.519(2)	2.5290(2)	2.535(2)	2.542(4)	2.552(2)

[a] Data from Ref. [5].

antiferromagnetic between planes along the *c*-axis [5]. A similar structure could be present here; however, additional measurements would have to be performed to verify the magnetic structure.

The field-dependent magnetization for H along the *c*-axis is shown in Fig. 3a. At low fields (<~1 T) the magnetization increases linearly with field, consistent with a slight spin canting along the *c*-axis. However, near $H \sim 3$ T, we observe a sudden change in slope associated with a metamagnetic transition that is slightly hysteretic. The metamagnetic transition is consistent with those observed for Ln_2MGa_{12} (Ln = Ce–Nd, M = Pd, Ni, and Cu) and is reminiscent of a spin-flip transition from an antiferromagnetic state at low fields to a spin re-orientation at higher applied fields [5,7,8], i.e. in this case, an abrupt aligning of all the spins along the *c*-axis. The saturated magnetic moment ($M \sim 1.7\mu_B$/Pr) is well below that expected for free Pr^{3+} ions, $\mu_{sat} = 3.20\mu_B$/Pr, indicative of a strong crystal electric field. The field-dependent magnetization for H along the *ab*-plane is shown in Fig. 3b. In this direction, the magnetization increases linearly with field and no metamagnetic transition is present.

Fig. 2a and b shows the temperature dependent molar magnetic susceptibility of Nd_2PdGa_{12} down to 3 K with the magnetic field applied along *c*-axis and *ab*-plane, respectively. With the field parallel to the *c*-axis, Nd_2PdGa_{12} undergoes an antiferromagnetic transition at 7.5 K with $H = 0.1$ T. However, in the *ab*-direction, no transition is observed. The inverse molar magnetic susceptibility (not shown) is consistent with Curie–Weiss like behavior at temperatures greater than 30 K, and fitting above this temperature with a modified Curie Weiss equation resulted in $\theta_W = -7.3(4)$ K along the *c*-axis and $\theta_W = -13.3(7)$ K along the *ab*-plane, as would be expected for antiferromagnetic coupling. The magnetic moment of $3.51(3)\mu_B$/Nd (along *c*) is in close agreement with the calculated moment of $3.62\mu_B$ for a free Nd^{3+} ion, while in the *ab*-direction the magnetic is slightly smaller at $3.32(1)\mu_B$/Nd. The field dependent magnetization of Nd_2PdGa_{12} with the field along the *c*-axis is shown in Fig. 3a. A sudden change in slope associated with a metamagnetic transition is observed at $H \sim 3$ T with a saturating magnetization of $\sim 1.6\mu_B$/Nd. The observed tendency toward saturation at $1.6\mu_B$/Nd is well below the expected calculated saturation moment of $3.27\mu_B$/Nd, indicative of strong crystal electric field effects. In the *ab*-direction (Fig. 3b) the magnetization increases linearly with H, and no metamagnetic transition is observed.

The inset of Fig. 2a shows the temperature dependent molar magnetic susceptibility of Sm_2PdGa_{12} with H parallel to the *c*-axis of the single crystal, and shows an antiferromagnetic transition at $T_N \sim 7.5$ K at $H = 4$ T. A broad curvature can be observed from the inverse molar magnetic susceptibility (not shown) most likely from van Vleck paramagnetism. Fitting above 30 K with a modified Curie–Weiss equation resulted in a $\theta_W = -21(1)$ K as would be expected for an antiferromagnetic material, and the effective magnetic moment of $0.58(2)\mu_B$/Sm is less than the calculated moment of $0.85\mu_B$ for a free Sm^{3+} ion. Unlike the Pr and Nd analogues, for Sm_2PdGa_{12} the temperature dependent molar magnetic susceptibility along the *ab*-plane (inset of Fig. 2b) shows an antiferromagnetic transition at 7 K. In this direction, the inverse molar magnetic susceptibility also shows curvature possibly due to van Vleck paramagnetism. Fitting the susceptibility above 30 K with a modified Curie–Weiss equation resulted in a $\theta_W = -16(1)$ K as would be expected for an antiferromagnetic material, and the effective magnetic moment of $0.67(1)\mu_B$/Sm again less than the expected for a free Sm^{3+} ion.

Field-dependent magnetization of Sm_2PdGa_{12} along the *c*-axis is shown in the inset of Fig. 3a and is linear at low fields then a change in slope occurs near 1 T before increasing linearly up to 9 T. With the field applied field in the *ab*-direction (Fig. 3b), the magnetization increases linearly with field. In both directions, the gradual linear increase in magnetization is consistent with the canting of antiferromagnetic spins. These results differ from Ce_2PdGa_{12}, Pr_2PdGa_{12}, and Nd_2PdGa_{12}, as these three analogues undergo metamagnetic transitions at $H \sim 3$ T. This behavior, coupled with the trend in θ_W,

Table 4
Magnetic properties.

Compound	Direction	θ	T_N	μ_{calc}	μ_{eff}	Fit temperature (K)
Ce_2PdGa_{12}[a]	$H\|\|c$	18.2	11	2.54	2.59	>100
Ce_2PdGa_{12}[a]	$H\|\|ab$	−14.8	–	2.54	2.54	>100
Pr_2PdGa_{12}	$H\|\|c$	10.1(1)	18.0	3.58	3.64(1)	>30
Pr_2PdGa_{12}	$H\|\|ab$	−21.5(1)	–	3.58	3.61(3)	>35
Nd_2PdGa_{12}	$H\|\|c$	−7.3(4)	7.5	3.62	3.51(3)	>30
Nd_2PdGa_{12}	$H\|\|ab$	−13.3(7)	–	3.62	3.32(1)	>40
Sm_2PdGa_{12}	$H\|\|c$	−21(1)	7.5	0.85	0.58(2)	>30
Sm_2PdGa_{12}	$H\|\|ab$	−16(1)	7	0.85	0.67(1)	>30

[a] Data obtained from Ref. [5].

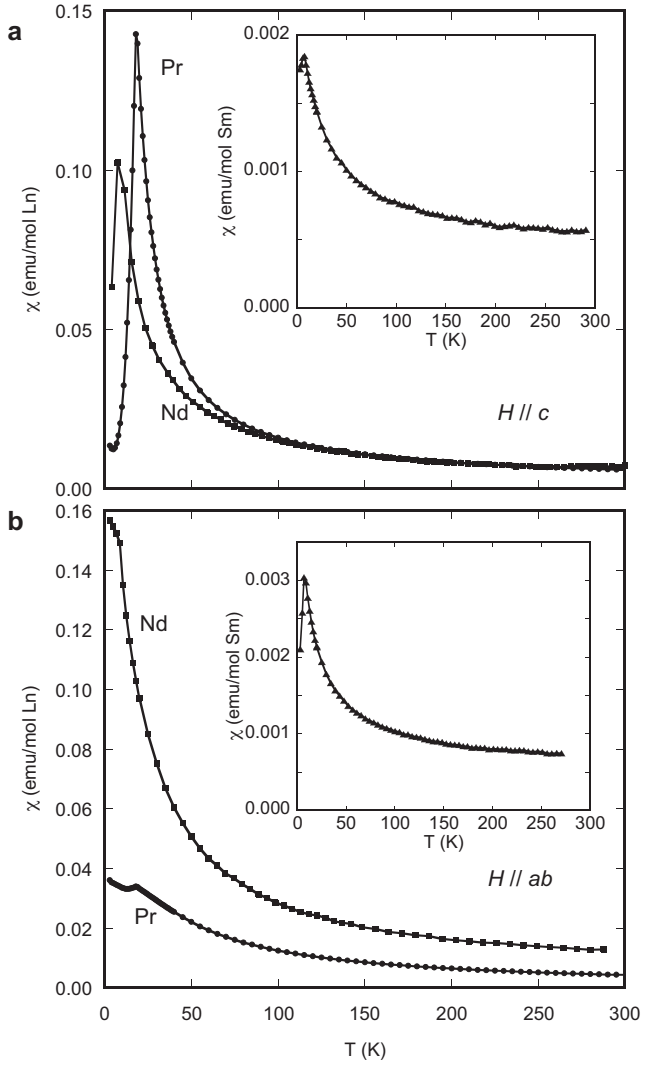

Fig. 2. (a) Molar magnetic susceptibility for Pr_2PdGa_{12} (circles) and Nd_2PdGa_{12} (squares) as a function of temperature measured under an applied field of 0.1 T ($H||c$). The inset shows molar magnetic susceptibility of Sm_2PdGa_{12} ($H||c$) (triangles) as a function of temperature measured under an applied field of 4 T. (b) Temperature dependent molar magnetic susceptibility for crystals oriented $H||ab$ for Pr_2PdGa_{12} (circles) and Nd_2PdGa_{12} (squares). The inset shows magnetic susceptibility for Sm_2PdGa_{12} (triangles) as a function of temperature.

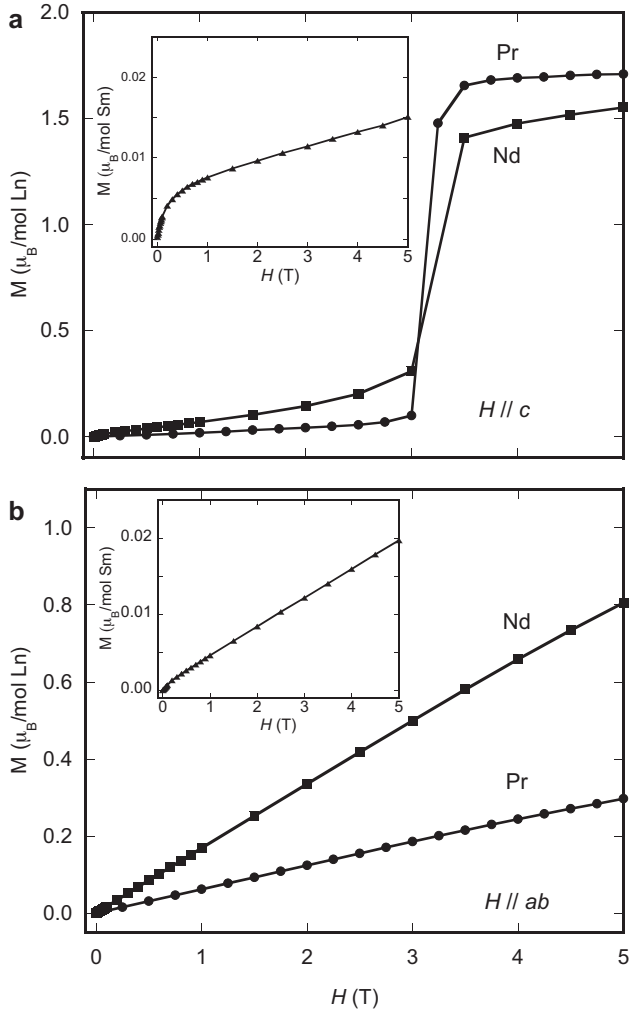

Fig. 3. (a) Magnetization of Ln_2PdGa_{12} as a function of applied field (parallel to the c-axis) at 3 K. (b) Magnetization of Ln_2PdGa_{12} as a function of applied field (parallel to ab-plane) at 3 K.

suggests that the lanthanide contraction is suppressing the magnetic anisotropy in these layered compounds.

3.2.2. Transport properties of Ln_2PdGa_{12} (Ln = Pr, Nd, and Sm)

Fig. 4a and b shows the heat capacity and entropy for Pr_2PdGa_{12} as a function of temperature, respectively. Two transitions are observed, T_1 and T_2, at 3.0 and 14.9 K, respectively. The second transition (T_2) at 14.9 K corresponds with the antiferromagnetic transition observed at 18 K in the molar magnetic susceptibility. The molar magnetic susceptibility was measured down to 3 K with only a slight upturn below 5 K. The T_1 transition could be magnetic in nature but lies just beyond the range of the collected magnetic susceptibility data. The sudden and dramatic upturn observed in the heat capacity data as $T \rightarrow 0$ is consistent with the hyperfine interaction. This interaction can result in a splitting of the six-fold degenerate nuclear states and give rise to a nuclear Schottky anomaly in $C(T)$ at 0.1 K of $\sim$7 J mol^{-1} K^{-1}. Phonon subtraction was achieved by the subtracting the nonmagnetic La_2PdGa_{12} analogue from the heat capacity data for Pr_2PdGa_{12}. Fitting this data over the range of $15.6 < T < 21.0$ K, the Sommerfeld parameter, γ, is 250 mJ mol^{-1} K^{-2} f.u. This indicates Pr_2PdGa_{12} may be a heavy fermion material. As can be seen in Fig. 4b, the recovered entropy is $\sim$0.87Rln3 at 15 K, and the expected full entropy of Rln3 is not recovered up to 20 K. We see no evidence for short-range order above T_c, and the effective moments obtained from susceptibility fits agree well with a Pr^{3+} ion. The saturation of the magnetization well below what is expected for a Pr^{3+} ion ($\mu_{sat} = 3.20\mu_B$/Pr), as shown in Fig. 3a, is indicative of strong crystalline electric field effects, which may account for the lower than expected magnetic entropy associated with $R\ln(2S+1)$. It is unclear if Pr_2PdGa_{12} is a heavy fermion, but the Kadowaki–Woods ratio, discussed below, is in agreement with previously published Pr-containing heavy fermions [11].

Resistivity data (Fig. 5) show metallic behavior for all three compounds for the entire temperature range investigated. The plot of resistivity vs. temperature for Pr_2PdGa_{12} shows some curvature near 100 K. Resistivity scales with T^2 for Pr_2PdGa_{12}, while Nd_2PdGa_{12} and Sm_2PdGa_{12} do not. Linear dependence of resistivity with T^2, shown as the inset of Fig. 5, is indicative of Fermi-liquid behavior and is common to many heavy fermion compounds, including the Pr-containing heavy fermion compounds $Pr_2Pd_3Ge_5$ [12] and $PrFe_4Sb_{12}$ (above its superconducting transition) [11]. However, the Pr heavy fermion $PrAg_2In$ does not show T^2 behavior [13]. Fitting the resistivity between 0 and 40 K to the equation $\rho = \rho_0 + AT^2$, yields an A-value of 0.0032(1) $\mu\Omega$ cm K^{-2}.

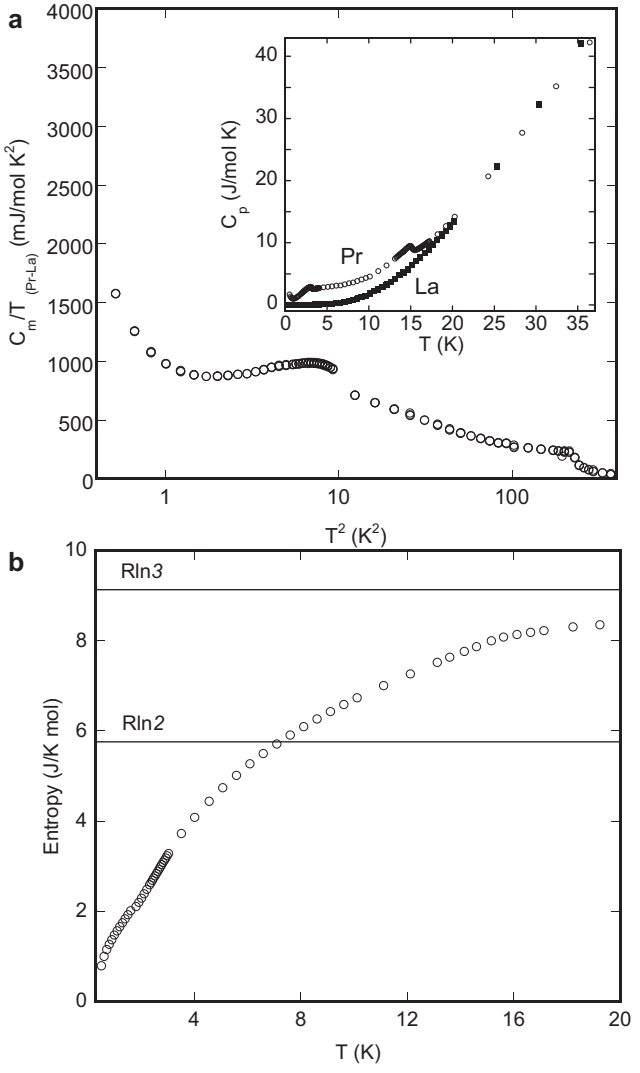

Fig. 4. (a) C_m/T vs. T^2 as obtained by subtraction of La_2PdGa_{12} from Pr_2PdGa_{12}. Inset shows C_p vs. T for both the La and Pr analogues. (b) Entropy vs. T as obtained from data shown in (a). *R*ln2 and *R*ln3 shown to guide expected S_{mag} contribution.

The Kadowaki–Woods ratio, A/γ^2, where A is the coefficient of the quadratic term of the low temperature resistivity, and γ is the electronic term from heat capacity can be used to characterize heavy fermion compounds. Using $\gamma \sim 250\,\mathrm{mJ\,mol^{-1}\,K^{-2}}$ gives a Kadowaki–Woods ratio of $\sim 5 \times 10^{-8}\,\mu\Omega\,\mathrm{cm\,mol^2\,K^2\,mJ^{-2}}$, which is approximately two orders of magnitude smaller than that expected for a heavy fermion compound, and more like that of a transition metal [20,21]. However, this is in excellent agreement with the praseodymium heavy system $PrOs_4Sb_{12}$ which gives a Kadowaki–Woods ratio of $\sim 4 \times 10^{-8}\,\mu\Omega\,\mathrm{cm\,mol^2\,K^2\,mJ^{-2}}$ [11]. This contrasts with praseodymium heavy systems $Pr_2Rh_3Ge_5$ and $Pr(CuGa)_{13-x}$ which have KW ratios of $\sim 4 \times 10^{-5}$and $\sim 0.7 \times 10^{-5}\,\mu\Omega\,\mathrm{cm\,mol^2\,K^2\,mJ^{-2}}$, respectively [10,12].

We have reported the single crystal growth of Pr_2PdGa_{12}, Nd_2PdGa_{12}, and Sm_2PdGa_{12} via the flux growth technique. Single crystals of all three phases were characterized by single crystal X-ray diffraction and their composition determined by SEM/EDXS analysis. Pr_2PdGa_{12}, Nd_2PdGa_{12}, and Sm_2PdGa_{12} order antiferromagnetically at 18, 7.5, and 7.5 K, respectively. Comparing all analogues of Ln_2PdGa_{12} (Ln = Ce, Pr, Nd, and Sm), θ becomes increasingly more negative as nearest neighbor distances decrease. This contrasts with the Ni and Cu analogues, where no clear trend can be observed in θ [8]. Both Pr_2PdGa_{12} and Nd_2PdGa_{12} undergo

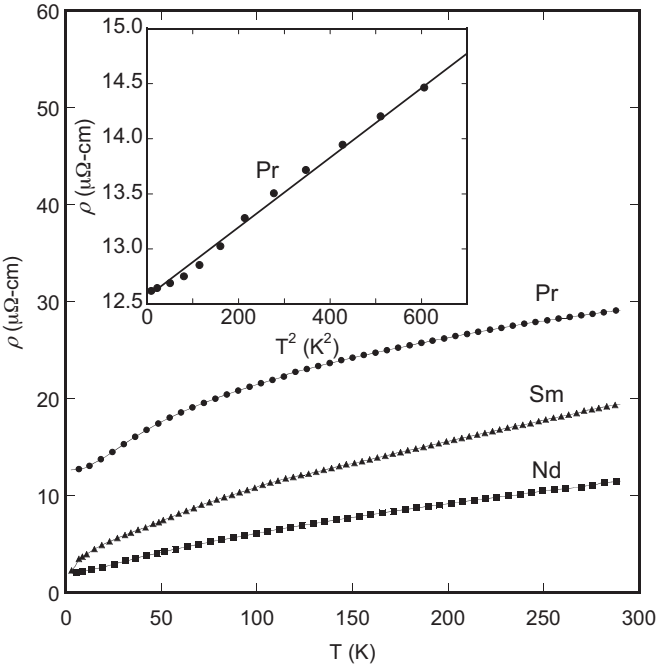

Fig. 5. Electrical resistivity data for Pr_2PdGa_{12} (circles), Nd_2PdGa_{12} (squares), and Sm_2PdGa_{12} (triangles). Inset shows T^2 dependence of resistivity for Pr_2PdGa_{12} fit over the range of $3 < T < 25$ K.

metamagnetic transitions with applied fields larger than 3 T, while Sm_2PdGa_{12} remains linear up to $H = 9$ T, consistent with related phases. Pr_2PdGa_{12} shows two transitions, T_1 and T_2, in the heat capacity at 3 and 15 K, respectively. The Sommerfeld parameter, γ, was determined to be $\sim 250\,\mathrm{mJ\,mol^{-1}\,K^{-2}}$ ($16 < T < 21$ K), and the Kadowaki–Woods ratio was consistent with that of $PrOs_4Sb_{12}$ [11]. Preliminary results support that Pr_2PdGa_{12} is a new Pr-containing heavy fermion, but experiments are warranted to elucidate the nature of the heavy electron state and the role of the crystal electric field in this system.

Acknowledgements

J.Y.C. acknowledges an NSF-DMR1063735 for partial support of this project. D.P.Y. acknowledges the support of the NSF under Grant No. DMR-1005764. We also thank Toshiro Sakakibara for useful discussions.

Appendix A. Supplementary data

Supplementary data associated with this article can be found, in the online version, at doi:10.1016/j.jallcom.2011.10.086.

References

[1] Y.N. Grin, Y.P. Yarmolyuk, E.I. Gladyshevskii, Sov. Phys. Crystallogr. 24 (1979) 137–139.
[2] C. Petrovic, et al., J. Phys.: Condens. Matter 13 (2001) L337.
[3] H. Hegger, C. Petrovic, E.G. Moshopoulou, M.F. Hundley, J.L. Sarrao, Z. Fisk, J.D. Thompson, Phys. Rev. Lett. 84 (2000) 4986.
[4] R.T. Macaluso, S. Nakatsuji, H. Lee, Z. Fisk, M. Moldovan, D.P. Young, J.Y. Chan, J. Solid State Chem. 174 (2003) 296–301.
[5] R.T. Macaluso, J.N. Millican, S. Nakatsuji, H.-O. Lee, B. Carter, N.O. Moreno, Z. Fisk, J.Y. Chan, J. Solid State Chem. 178 (2005) 3547–3553.
[6] J.N. Millican, R.T. Macaluso, D.P. Young, M. Moldovan, J.Y. Chan, J. Solid State Chem. 177 (2004) 4695–4700.
[7] J.Y. Cho, J.N. Millican, C. Capan, D.A. Sokolov, M. Moldovan, A.B. Karki, D.P. Young, M.C. Aronson, J.Y. Chan, Chem. Mater. 20 (2008) 6116–6123.
[8] K.R. Thomas, J.Y. Cho, J.N. Millican, R.D. Hembree, M. Moldovan, A. Karki, D.P. Young, J.Y. Chan, J. Cryst. Growth 312 (2010) 1098–1103.

[9] E.L. Thomas, J.N. Millican, E.K. Okudzeto, J.Y. Chan, Comments Inorg. Chem. 27 (2006) 1–39.
[10] J.Y. Cho, E.L. Thomas, Y. Nambu, C. Capan, A.B. Karki, D.P. Young, K. Kuga, S. Nakatsuji, J.Y. Chan, Chem. Mater. 21 (2009) 3072–3078.
[11] E.D. Bauer, N.A. Frederick, P.C. Ho, V.S. Zapf, M.B. Maple, Phys. Rev. B: Condens. Matter 65 (2002) 100506.
[12] V.K. Anand, Z. Hossain, C. Geibel, Phys. Rev. B: Condens. Matter 77 (2008) 184407.
[13] A. Yatskar, W.P. Beyermann, R. Movshovich, P.C. Canfield, Phys. Rev. Lett. 77 (1996) 3637.
[14] E.A. Goremychkin, R. Osborn, E.D. Bauer, M.B. Maple, N.A. Frederick, W.M. Yuhasz, F.M. Woodward, J.W. Lynn, Phys. Rev. Lett. 93 (2004) 157003.
[15] P.C. Canfield, Z. Fisk, Philos. Mag. B 65 (1992) 1117–1123.
[16] L.O. Vasilenko, A.S. Noga, Y.N. Grin, M.D. Koterlin, Y.P. Yarmolyuk, Russ. Metall. (1988) 216–220.
[17] A. Altomare, M.C. Burla, M. Camalli, G.L. Luca, C. Gaicovazzo, A. Guagliardi, A.G.G. Moliterni, G. Polidori, R. Spagna, J. Appl. Crystallogr. 32 (1999) 115.
[18] G.M. Sheldrick, Acta Crystallogr. A 64 (2008) 112–122.
[19] X.Z. Chen, P. Small, S. Sportouch, M. Zhuravleva, P. Brazis, C.R. Kannewurf, M.G. Kanatzidis, Chem. Mater. 12 (2000) 2520–2522.
[20] K. Kadowaki, S.B. Woods, Solid State Commun. 58 (1986) 507–509.
[21] A.C. Jacko, J.O. Fjaerestad, B.J. Powell, Nat. Phys. 5 (2009) 422–425.